Advanced Composite Materials
Publication details, including instructions for authors and subscription information:
http://www.tandfonline.com/loi/tacm20

Bond Strength of Carbon Fiber Sheet on Concrete Substrate Processed by Vacuum Assisted Resin Transfer Molding

N. Uddin [a] , M. Shohel [b] , U. K. Vaidya [c] & J. C. Serrano-Perez [d]

[a] Department of Civil and Environmental Engineering, The University of Alabama at Birmingham, 1075 13th Street South, Birmingham, Alabama 35294-4440, USA;, Email: nuddin@uab.edu

[b] Department of Civil and Environmental Engineering, The University of Alabama at Birmingham, 1075 13th Street South, Birmingham, Alabama 35294-4440, USA

[c] Department of Materials Science and Engineering, The University of Alabama at Birmingham, Birmingham, Alabama 35294, USA

[d] Department of Materials Science and Engineering, The University of Alabama at Birmingham, Birmingham, Alabama 35294, USA

Version of record first published: 02 Apr 2012.

///VSP///

Advanced Composite Materials 17 (2008) 277–299

ADVANCED COMPOSITE MATERIALS
www.brill.nl/acm

Bond Strength of Carbon Fiber Sheet on Concrete Substrate Processed by Vacuum Assisted Resin Transfer Molding

N. Uddin [a,*], **M. Shohel** [a], **U. K. Vaidya** [b] **and J. C. Serrano-Perez** [b]

[a] Department of Civil and Environmental Engineering, The University of Alabama at Birmingham, 1075 13th Street South, Birmingham, Alabama 35294-4440, USA

[b] Department of Materials Science and Engineering, The University of Alabama at Birmingham, Birmingham, Alabama 35294, USA

Received 19 February 2004; accepted 25 January 2008

Abstract

High quality and expedient processing repair methods are necessary to enhance the service life of bridge structures. Deterioration of concrete can occur as a result of structural cracks, corrosion of reinforcement, and freeze–thaw cycles. Cost effective methods with potential for field implementation are necessary to address the issue of the vulnerability of bridge structures and how to repair them. Most infrastructure related applications of fiber-reinforced plastics (FRPs) use traditional hand lay-up technology. The hand lay-up is tedious, labor-intensive and relies upon personnel skill level. An alternative to traditional hand lay-up of FRP for infrastructure applications is Vacuum Assisted Resin Transfer Molding (VARTM). VARTM uses single sided molding technology to infuse resin over fabrics wrapping large structures, such as bridge girders and columns. There is no work currently available in understanding the interface developed, when VARTM processing is adopted to wrap fibers such as carbon and/or glass over concrete structures. This paper investigates the interface formed by carbon fiber processed on to a concrete surface using the VARTM technique. Various surface treatments, including sandblasting, were performed to study the pull-off tensile test to find a potential prepared surface. A single-lap shear test was used to study the bond strength of CFRP fabric/epoxy composite adhered to concrete. Carbon fiber wraps incorporating Sikadur HEX 103C and low viscosity epoxy resin Sikadur 300 were considered in VARTM processing of concrete specimens.

Keywords

VARTM, FRP reinforcement, RC beams

1. Introduction

The epoxy bonded FRP system has proven its potentiality to retrofit structurally deficient concrete structures [1–4]. Most of the works that have been done up to the present time are based on a common traditional method for bonding the

* To whom correspondence should be addressed. E-mail: nuddin@uab.edu
Edited by JSCM

DOI:10.1163/156855108X345199

FRP on concrete surface. Little or no special attention has been paid to improving the quality of the interfaces developed in the traditional processing techniques. A weak interface, produced from various defects during the processing of composite laminates/fabrics, creates potential problems, such as water seepage, fiber wrinkling, premature failure of beam caused by de-bonding at the interface and moisture-induced delamination. A high quality processing technique is essential for successful composite part fabrication for retrofitting purposes. There are four basic steps involved in a composite manufacturing process: wetting/impregnation, lay-up, consolidation, and solidification. In order to avoid process-related defects, each of the above basic steps should be well handled to achieve high product quality and reliability. Especially consolidation is a very important step in obtaining a good quality part as it creates the intimate contact between concrete substrata and each layer of prepreg or lamina. A poorly consolidated part will have voids and dry spots. As an alternative to the labor intensive hand lay-up process, VARTM is an attractive process since it can save processing time (especially when many FRP layers are being applied), makes the resin application more uniform than with traditional hand lay-up, and has also proven to be environmentally friendly since it has zero volatile organic compound (VOC) emissions. It is a process widely used in automotive and aerospace applications. The shortcomings of traditional lay-up techniques are: (a) the need for skilled workers to handle the fabric; (b) improper wetting; (c) difficulty to controlling the process in long bridge girders and columns. On the other hand, VARTM is believed to form a strong uniform interface, free of resin-rich areas, without compromising the integrity of the fabric.

2. Literature Survey

Substantial experimental and theoretical work exists on the bond strength of FRP to concrete. Experiments have been carried out using several set-ups, including single shear tests, double shear tests, and modified beam tests. Chajes *et al.* [5] studied the bond and force transfer mechanism in composite material plates bonded to concrete, using a single-lap shear test specimen. Test results showed that (1) surface preparation of the concrete can influence the bond strength, (2) if the failure mode of the joint is governed by shearing of the concrete, the ultimate bond strength will be proportional to the square root of concrete compressive strength f'_c, (3) there is an effective bond length for a joint beyond which no further increase in failure load can be achieved. A group of researchers conducted a study on the effect of the type of concrete surface preparation on the bond of carbon FRP (CFRP) sheets [6]. The bonded length of the CFRP sheet was determined to have little effect on the ultimate load of the specimen. Another group of researchers studied the effect of test method and quality of concrete on the bond of CFRP sheets [7]. Three failure modes were observed: shearing of the concrete, delamination and FRP rupture. Brosens and Van Gemert [8] performed direct shear tests on two concrete prisms connected with three layers of CFRP on two opposite sides. They concluded that

for computational purposes a linear bond stress distribution in the FRP sheet may be assumed. Another study on the bond mechanism of CFRP sheets was conducted by Maeda *et al.* [9]. Results of the tests showed that, as the stiffness of the fiber sheet increases, the ultimate load increases.

Xie and Kharbari [10] used a specially designed peel test to characterize the bond strength between a carbon fiber/epoxy composite and a concrete substrate. They observed that cohesive debonding in the concrete substrate is the least likely failure mode. However, for a small peel angle the difference is small and cohesive failure in the concrete is more likely than for a larger peel angle. Täljsten [11, 12] carried out shear tests on concrete prisms with steel and CFRP bonded plates. Results were compared with Volkersen's theory [12] for lap joints and the comparison showed that the theory can predict the shear stress in the joint fairly well for moderate load levels. Bizindavyi and Neale [13] performed an experimental and analytical investigation on transfer lengths and bond strengths of composite laminates bonded to concrete. The observed modes of failure were shearing of the concrete beneath the glue line and rupture of the composite coupon. An analytical model based on a shear lag approach was developed. Volnyy and Pantelides [14] investigated the bonding between concrete and CFRP plates to be used as connections in precast concrete walls. Failure occurred in all specimens due to one, or a combination, of the following modes: CFRP rupture, delamination of the CFRP from the concrete and concrete surface shear failure.

Nanni *et al.* [15] developed a bond model for the failure load and the effective bond length for FRP laminates to concrete substrate. A shear lag approach, along with a simple shear model for the evaluation of the slip modulus, was used to model the strain distribution at moderate load levels. Chen and Teng [16] studied a simple and rational bond strength model based on existing fracture mechanics analysis and experimental observation. They designed an anchorage length so that the full tensile strength of the reinforcement can be achieved.

Wu *et al.* [17] introduced a nonlinear fracture mechanics approach to derive theoretical solutions for the interfacial stress transfer of an adhesive pull–pull bonded joint by comparing with the case of a pull–push bonded joint. The nonlinear behavior was modeled by using two kinds of assumed shear stress-slip curves. The numerical simulations indicated that this method can be used to predict fracturing procedures such as initiation of interfacial microcracking and macrocracking/debonding, cracking propagation, shear stress distribution, and load-carrying capacity along FRP–concrete/FRP–steel/steel–concrete interfaces.

3. Experimental

3.1. Bond Mechanism and Adhesion in Concrete–FRP Interface

Adhesion, in terms of concrete, resin and FRP reinforcement, is defined by Karbhari *et al.* [18] as the level of attraction between two substrates. It can be created by a number of mechanisms including: mechanical interlocking, diffusion theory,

Figure 1. Appearance of average as cast surface 55 MPa concrete.

electronic theory and absorption theory. In the case of the concrete–FRP interface, the dominant mechanism of adhesion is the mechanical interlocking of the resin in the irregularities of the concrete surface. From this information it can be inferred that a rougher surface can provide better interlocking between the resin and the concrete and thus a stronger interface. However, the exact limits for how rough a surface should be are not yet available in practice, and it has been proven in certain studies that excessive roughness [19] can induce out of plane stresses that actually cause more damage than helping the concrete–FRP interface.

3.1.1. Studies on the Surface Preparation of Concrete

Surface preparation techniques were reviewed and analyzed to investigate the sensitivity of the interface between CFRP and concrete. In order to understand the surface strength of concrete and its possible role in the debonding characteristics of CFRPs, different surface preparation techniques were reviewed and analyzed to investigate the sensitivity of the interface to the effects of surface preparation. As-cast concrete (Fig. 1) has a general characteristic that may not be adequate if used as a substrate. The weak mortar layer that is exposed in the outer surface of concrete represents a potential problem if it is not removed from the concrete prior to retrofitting. This is the one of the main causes of premature delamination of the fabric wrap, and in practice limits the performance of the CFRP reinforcement by a great percentage.

The correct preparation of the concrete surface is vital in developing a strong interface between the concrete and the carbon fiber sheet/fabric. Prior studies of surface preparation by Toutanji and Ortiz [20] have proven the importance of surface preparation. The use and selection of a proper method for preparing the surface of the specimens was conducted in compliance with the following rules. First, the chosen surface preparation technique should generate a very strong contact surface that will assure that the weak layer of mortar in the surface will be removed, exposing the aggregate. Secondly, the technique should generate the maximum interfacial area possible, so as to increase the contact area, which is generally diminished by the pores present in the surface after sand blasting or any other means of surface

layer removal. The third condition for the selection of a surface preparation method is that it should be as economically attractive and less labor intensive as possible. Representative prism specimens were pre-treated by sandblasting, wire brushing, and a regular as-cast surface. The pull-off test (ACI-503R, ASTM C 4541) was conducted in order to quantify the resultant surface strength of concrete in each case and to analyze which one resulted in a better surface strength. The concrete test specimens used were made out of concrete with compressive strengths ranging from 24 to 65 MPa. After the surface is sandblasted with a pressure of 137 kPa, the overall roughness and porosity of the surface of concrete is enhanced, as seen in Fig. 2.

The difference is not as visually dramatic for the 55 MPa concrete. But the difference is significant in the 24 MPa concrete, as shown in Figs 3 and 4. Surface strength of concrete is not a material constant; its value can vary even for concrete mixed from the same batch. In order to get a reasonable result, several specimens have to be tested. The failure in the surface of concrete is often initiated by the voids of air formed inside the concrete during solidification. These air voids as seen in Fig. 5 reduce the overall area being loaded and eventually facilitate failure. The scanning electron microscopy (SEM) image taken of a failed specimen from the

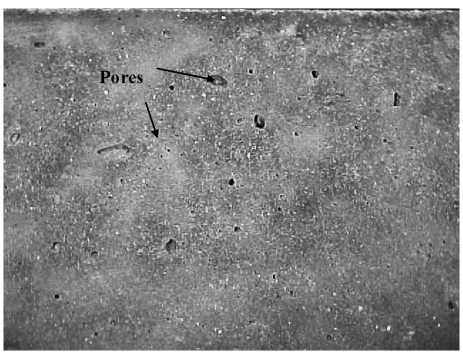

Figure 2. Surface appearance of 55 MPa concrete after sandblasting.

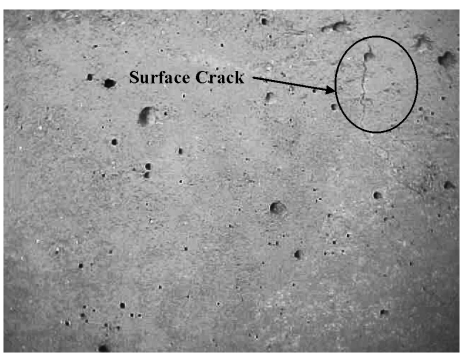

Figure 3. Surface appearance of 24 MPa concrete before sandblasting.

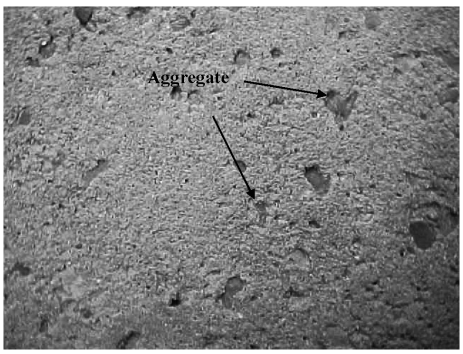

Figure 4. Surface appearance of 24 MPa concrete after sandblasting at 137 kPa.

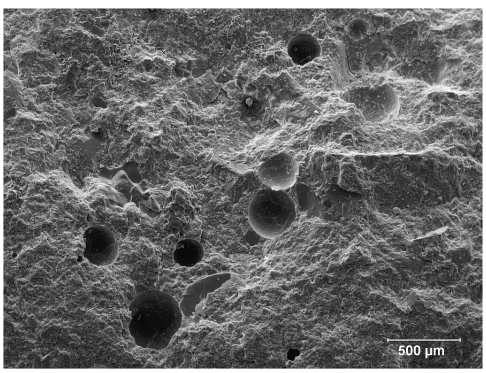

(a)

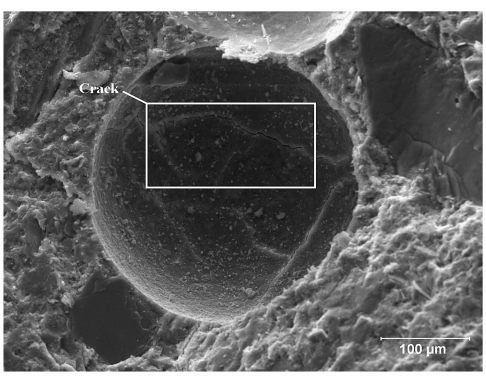

(b)

Figure 5. (a) Air inclusions in concrete specimen failed by pull-off test; (b) micro cracks inside inclusion.

pull-off test reveals the importance of the number of air voids inside the concrete substrate and their role in the pull-off test fracture. Since the average number of air voids, and the amount and size of aggregate particles in a certain zone is not a fixed parameter, the value for the overall surface strength is always an approximation.

For the following testing, the values used for the surface tensile strength represent an average value of the samples tested at our laboratory.

3.1.2. Pull-off Test Results

Concrete prisms as-cast, sandblasted, and wire brushed were cleaned by compressed air first and then treated with a layer of epoxy resin. Following the procedure from ACI 305R, a 50.8 mm (2″) aluminum disc was bonded to the surface, and then attached to the testing machine (DYNA Pull-off Tester), which gradually increased the tensile load until failure. The pull-off test machine is shown in Fig. 6. The results of pull-off tests are plotted in Fig. 7. For comparison purposes, the concrete splitting tensile strength f_{ct} given by

$$f_{ct} = 0.53 * \sqrt{f'_c} \tag{1}$$

was used. This equation obtained from Teng *et al.* [21] (2002) was developed based on the concrete compressive strength f'_c.

There is a noticeable change in surface strength from the as-cast specimen to the sandblasted surface. It could be that the sandblasting is responsible for the increase in surface strength up to a limit and that the exposed aggregate also plays an im-

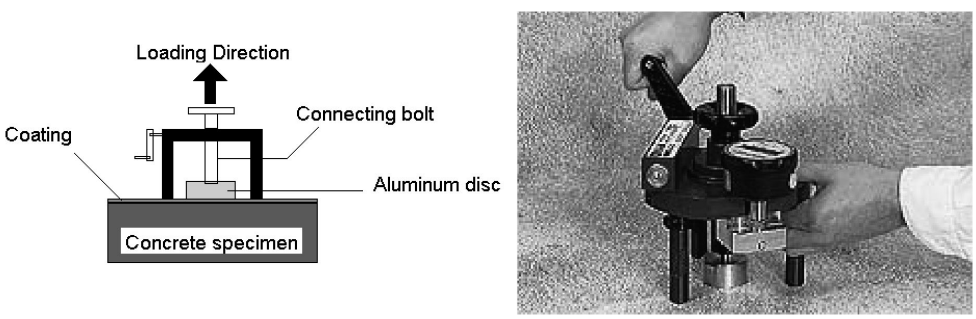

Figure 6. Pull-off test schematic and machine.

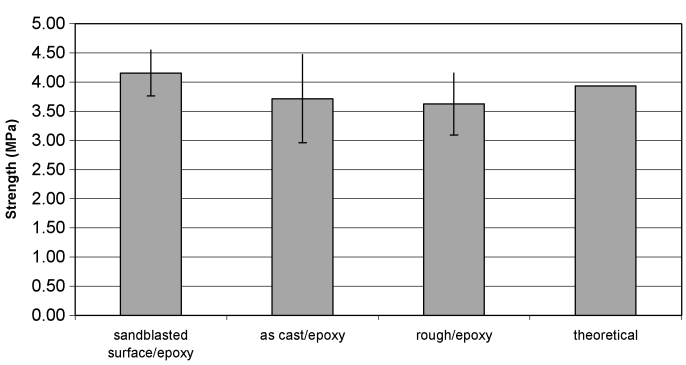

Figure 7. Mean values of surface strength of concrete after different treatments obtained by pull-off test.

Figure 8. Failed specimen showing split aggregate and resin filled air-inclusions.

portant role in the process. Combined failure modes were encountered in testing, including different percentages of the following:

– Failure of the adhesive: separation from the epoxy and the concrete surface.

– Surface failure of the concrete: showing split aggregates and mortar on the disc.

From the graph of Fig. 7, it can be seen that the sandblasting improves the result from the pull-off test, and that exaggerated roughness (as in rough/epoxy sample) obtained through wire brushing does not necessarily contribute to better bonding [19]. The desired mode of failure in a pull-off test specimen can be observed in Fig. 8, showing mostly concrete failure, proving a very strong interface.

3.2. VARTM Process

Generally VARTM involves the following steps:

- Dry reinforcements (fibers/fabrics, cores performs, etc.) are placed in a one-sided, open mold.
- The lay-up is covered with an impervious bag, sealed, and placed under vacuum.
- One or more resin fill lines that feed into the bag are opened, and a low-viscosity resin impregnates the dry lay-up.
- After filling, the resin gels and cures.
- The bag is removed.

The general VARTM schematic is shown in Fig. 9.

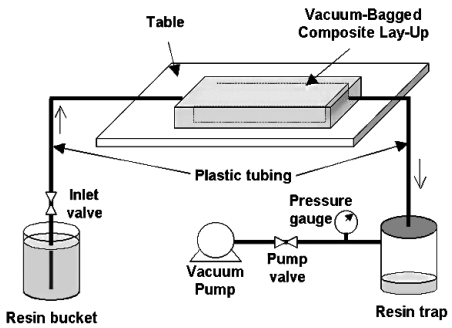

Figure 9. Schematic of VARTM.

3.2.1. VARTM in Concrete Prism

For VARTM application on concrete, the surface of the concrete acts as a tool for the infusion process. After the surface of the concrete is prepared, a layer of primer is applied in the area to be infused. A vacuum seal is formed around the concrete prism specimens, using vacuum bag sealant tape to ensure an airtight seal. The dry fabric, cut to shape is then placed on the concrete surface and held in place using adhesive tape on the edges. The stretched fabric is covered using a porous medium and a distribution mesh, to allow resin flow through the fabric. The location of infusion and vacuum lines are carefully designed and placed, and finally covered by a bagging film. The lay-up is kept under vacuum; the resin/hardener mixture is infused with the aid of the vacuum.

The resin flows across the fabric, and fills any surface flaws with the aid of the hydrostatic pressure that is applied by the atmosphere on the bag. The infusion parameters were optimized [21] according to the equation (2) with φ porosity of the reinforcement, κ permeability of the reinforcement, η viscosity of the resin, l flow distance (length of the strip), ΔP applied pressure difference (constant during the injection), so that the infusion was symmetrical and even, and resin rich areas were avoided. Curing took place under vacuum:

$$\text{Fill-time} = \frac{\varphi \eta l^2}{2\kappa \Delta P}. \tag{2}$$

The filling time is directly proportional to the resin viscosity, low viscosity resin; Sikadur 300 (300 mPa s) was used. Most reinforcement permeability and porosity measurements vary between 0.5 and 0.85. A distribution medium was therefore used to optimize the overall permeability and porosity, and improve the fill time. The maximum infusion length was 30 cm in this case.

3.3. Bond Strength Studies

There is no work currently available that aids in understanding the interface that develops when VARTM processing is adopted to wrap fibers such as carbon and/or glass over concrete structures. This paper investigates the interface formed by carbon fiber processed onto a concrete surface using the VARTM technique, and

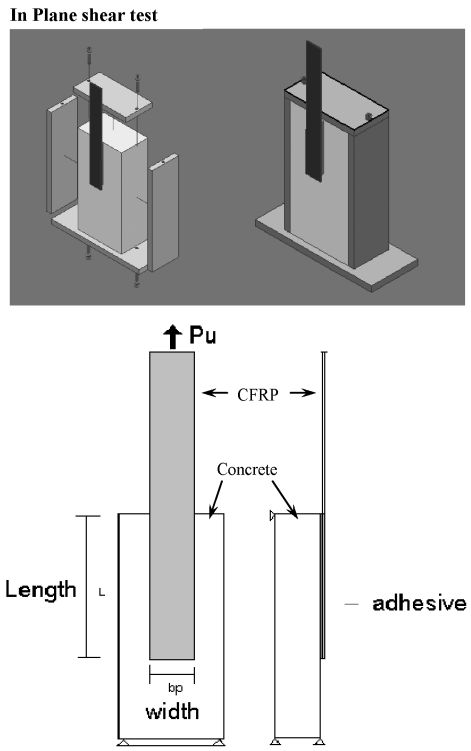

Figure 10. In-plane shear test schematic.

attempts to analyze the results based on the model of in-plane shear used by Bizindavyi and Neale [13]. This model offers an adequate way to determine the conditions at the interface between the composite and concrete as well as the general properties and behavior of the formed interface under the chosen conditions of surface preparation and processing. The main idea of this type of single lap shear test is to apply uniaxial tension on the fabric bonded to the concrete, so that the interface is subjected to shear focusing on both bond strength and forcing transfer. It is known that the application of a laminate to a concrete beam introduces shear transfer to the concrete/epoxy interface while the beam is loaded in flexure [22]. In general, the single-lap shear is easy to fabricate and proven to yield consistent values of average shear stress at failure (failure load divided by the bond area). The test setup is shown schematically in Fig. 10.

3.3.1. Specimens, Processing and Instrumentation

The specimens used were concrete prisms (40.64 cm × 7.62 cm × 10.16 cm) ranging in compressive strengths from 42 to 65 MPa. The samples were cast using a mix designed to produce 55 MPa concrete. The prisms were wet cured for 28 days by submerging them in a water tank. The surface of the prisms was sandblasted and primed according to the chosen surface treatment. A 2.54 cm wide and 38.1 cm long strip of Sikawrap HEX 103C was bonded to the surface with Sikadur 300 epoxy

Figure 11. Sample set for in-plane shear test.

Table 1.
Material properties, Sika construction product catalog [24]

Concrete		Adhesive (Sikadur 300)		CFRP (Sikawrap HEX 103C)	
Compressive strength f'_c	55 MPa	Tensile strength	64.8 MPa	Tensile strength	3.8 GPa
		Tensile modulus	2.06 GPa		
E	30.79 GPa	Shear strength	32.4 MPa	Tensile modulus	234.4 GPa
		Shear modulus	0.73 GPa		
Poisson's ratio	0.15	Poisson's ratio	0.4	Poisson's ratio	0.214

Table 2.
Cured laminate properties with Sikadur Hex 300 epoxy properties after standard cure, Sika construction product catalog [24]

Property	Design value
Tensile strength	717 (MPa)
Tensile modulus	65.087 (GPa)
Tensile % Elongation	0.98

resin leaving a free end of 19 cm, as seen in Fig. 11. Table 1 presents the material properties of fiber and resin, and Table 2 lists the cured laminate properties. The strip was bonded to the concrete both by VARTM and hand lay-up process. A total of 12 samples (6 using VARTM and 6 using hand lay-up process) were prepared for testing. In VARTM, the prism surface was vacuum bagged using the same process described in Section 3.2.1. After the epoxy cured, glass–epoxy tabs were bonded

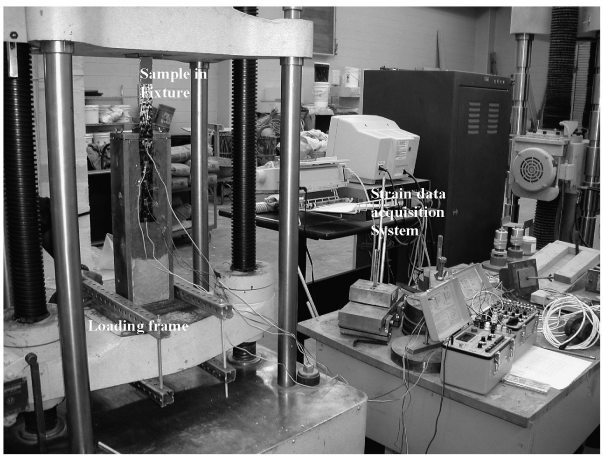

Figure 12. In-plane test set up.

to the top of the strip to firmly grip the FRP strip in the fixed cross-head of the 60 kips Tinus Olsen testing machine. The specimen was instrumented by connecting five strain gages to the surface of the fabric before placing into the testing machine as shown in Fig. 12. The strain gages were strategically placed, each spaced 2.5 cm starting from the edge of the concrete surface. The strain gages were then hooked up into the strain data acquisition system. The specimens were loaded monotonically to failure.

3.3.2. Bond Strength Test Results

Interface Developed Through VARTM Process. The specimens prepared using VARTM process were placed in the loading frame and loaded, and strain data were recorded. The typical strain distributions are shown in Fig. 13 (only four samples are presented for the sake of brevity; see Serrano-Perez 2003, Ref. [24], for details) up to a load close to failure. For all the specimens, the strain distribution shows linear curve both at the early stage of loading and ultimate loading (except specimens 2 and 3; they show a bilinear curve at the ultimate loading). It can be considered that failure occurs in the area between 0 and 25.4 mm for all the specimens. At ultimate loading, the applied load is sustained by the bond stress between concrete and FRP in the area beyond 25.4 mm.

As shown in the figure, the shear flow in the area between 0–25.4 mm is very high for all loading cases. Therefore the strain gradient is high in this region. For early stages of loading, strain reading was not observed at strain gage locations beyond 25.4 mm. For the area between 25.4 and 50/75 mm, very little or no strain was observed for 445 and 2224 N loading but a strain reading was noted at 4448 N loading. However, no strain reading was observed at or beyond the 100 mm length. The interface developed at failure (as seen in Fig. 14) represents a homogenous interface indicating a uniform load transfer through the interface.

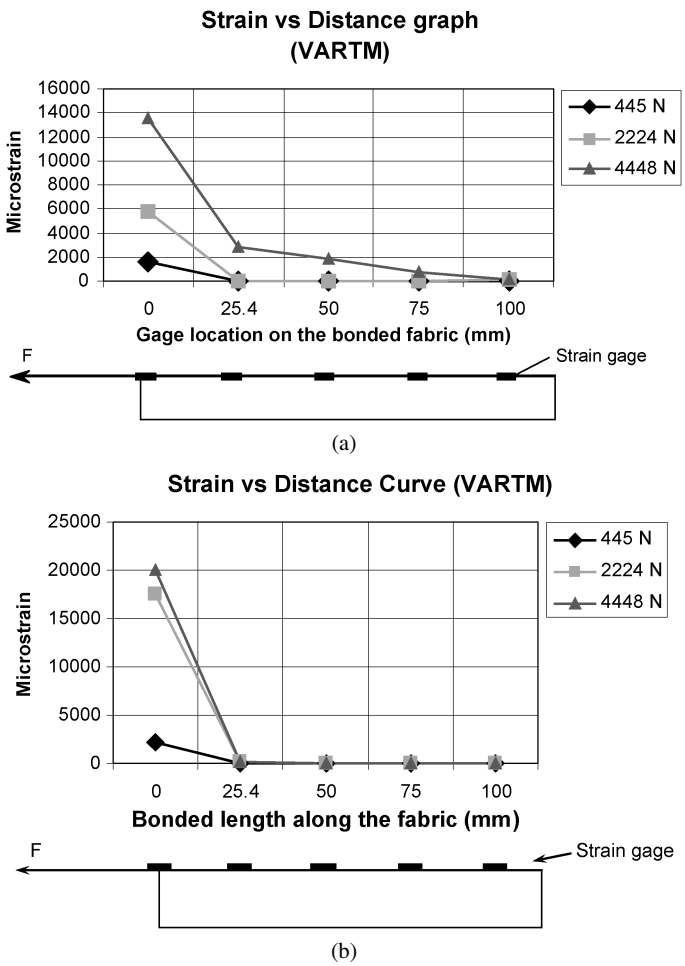

Figure 13. Typical strain profile in CFRP bonded to concrete substrate by VARTM, loaded in-plane.

Interface Developed in Hand Lay-up Process. A comparison study was done to investigate the interface developed by hand lay-up. Strain profiles for four hand lay-up specimens are shown in Fig. 15. For all the specimens, the strain distribution shows a linear curve at the early stage of loading. However, at ultimate loading the strain distribution is consistently bilinear.

When the applied load is 4.45 kN, the strain in the area between 0 and 25 mm becomes rather uniform, and a linear distribution is observed in the area between 25 and 75 mm. It can be considered that failure occurs in the area between 0 and 25 mm. At ultimate loading, the applied load is sustained by the bond stress between concrete and CFRP in the area beyond 100 mm. It can be considered that failure occurs in the area between 0 and 25.4 mm. At ultimate loading, the applied load is sustained by the bond stress between concrete and FRP in the area beyond 25.4 mm. At the early stage of loading, the load is sustained in the vicinity of loading point.

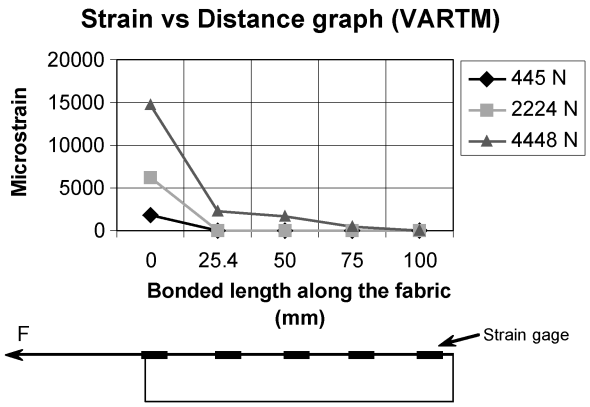

(c)

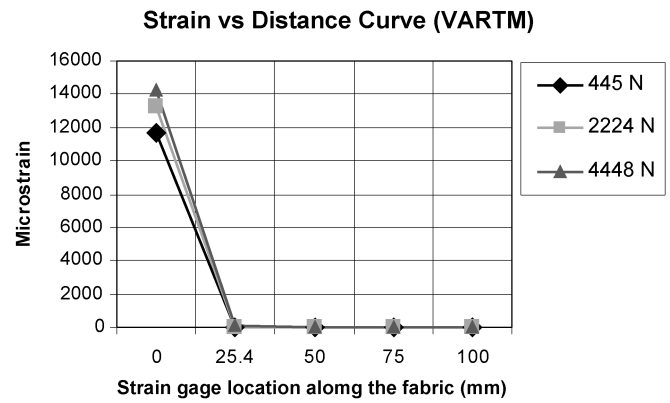

(d)

Figure 13. (Continued.)

If failure occurs in the vicinity due to fracture of the concrete surface, the area for active bonding is shifted to a new area. This phenomenon is repeated until failure propagates completely. At any stage of loading, the area where FRP resist through bond stress is a part of the bonded area of FRP.

Discussion. As observed in the VARTM and hand lay-up processed specimens, distinct patterns of strain regions could be identified depending on the level of applied loading. In the area between 0 and 25.4 mm, the strain rate is consistently lower in the hand lay-up processed specimens compared to VARTM. This was observed for all hand lay-up specimens. In addition, significant strain was observed in strain gage locations of hand lay-up processed specimens in the area between 25.4 and 50 mm whereas the strain is very little or zero for the VARTM processed specimens.

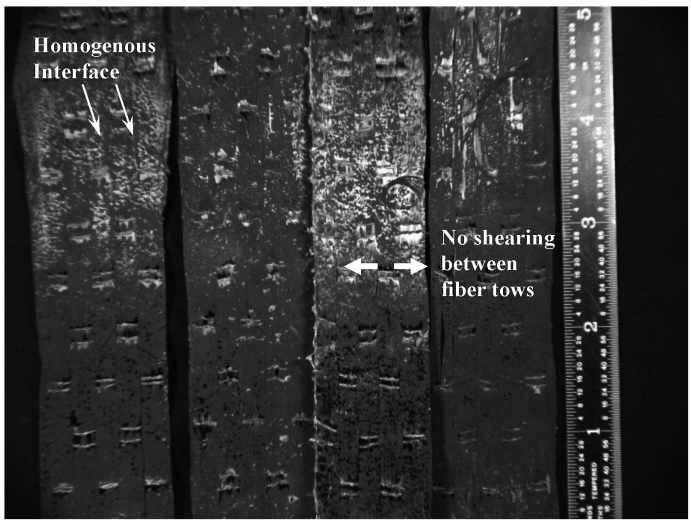

Figure 14. Interfaces obtained in VARTM after in-plane test. Observe a more homogeneous interface, no shearing between fiber tows.

On the other hand, the ultimate load for both VARTM processed and hand laid up processed specimens are very close as shown in Table 3. Accordingly much higher level of strains is observed in the VARTM processed specimens as high as 15 000 micro strains. It is clear that depending on the applied load, the strain is transferred through the bonded joint until failure occurs in a brittle manner when the interface fails in shear. In most of the hand lay-up processed specimens, failure was in the form of shear failure between the fiber tows as seen in Fig. 16. As shown in the figure, high resin rich areas are wide spread throughout the interface. In addition, high shear is evident between fiber tows causing tow separation. All these could be attributed to a non-homogeneous interface caused by poor consolidation typical of a hand lay-up process. Note that consolidation is a very important step in obtaining a good quality part as it creates the intimate contact between concrete substrata and each layer of the prepreg or lamina. A poorly consolidated part will have voids and dry spots, which may lead to a non-uniform load distribution within the fabric. The interface in VARTM, however, is homogeneous without any evidence of resin-rich areas and tow separation, as seen in Fig. 14. Moreover, failure modes encountered in the interface formed by VARTM show a uniform interface and cohesive failure without compromising the integrity of the fabric as encountered in the hand lay-up (Fig. 14 *vs* Fig. 16).

3.3.3. Bond Strength Model for VARTM Processed Specimens

It is observed from the strain profile of VARTM processed specimens (Fig. 13) that bond becomes fully developed in only at the first loaded zone of the interface as shown in the Fig. 17. This first loaded zone length is primarily responsible for transferring the entire load in this case, whereas for the hand lay up process speci-

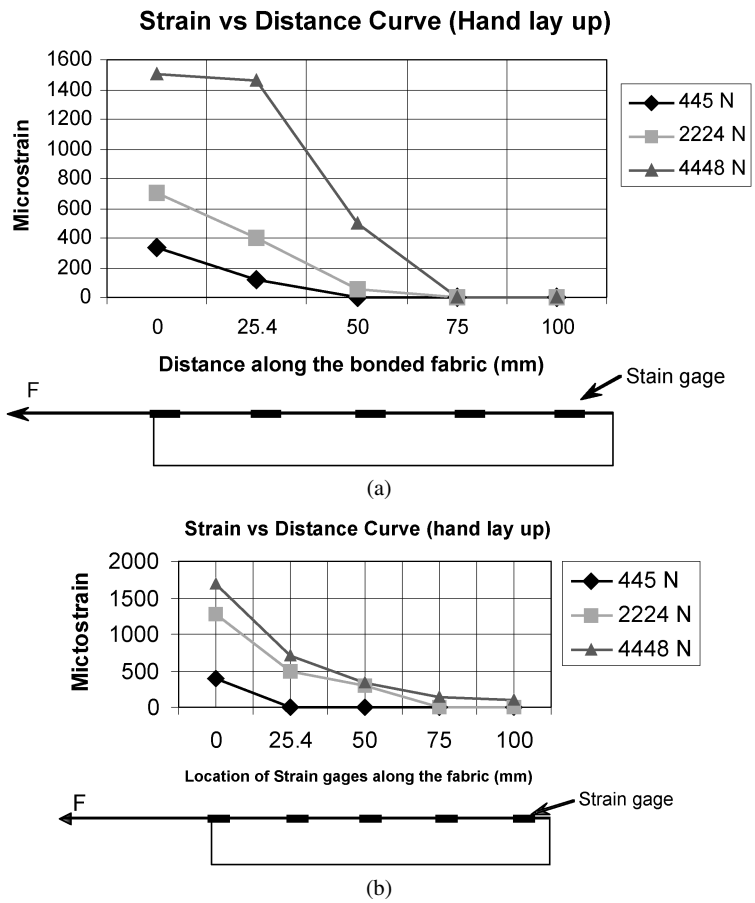

Figure 15. Typical strain profile for the in-plane shear test specimens processed by hand lay-up.

mens loaded zone continues up to 4th loaded zone (Fig. 15). This bond length can therefore be thought as a characteristic bond length in VARTM processing FRP specimens. Moreover the strain distribution is also not quite similar as observed in the hand lay-up processed specimen.

A comparison of the existing bond model available in the literature is presented in Fig. 18. As shown in the figure, each existing model either over predicts or under predicts the bond strength developed in the VARTM process. Any bond strength model adjusted for the hand lay up specimens therefore should be adjusted for VARTM processed specimens. Load transfer phenomena developed in VARTM process can be understood as follows.

The interface developed during the VARTM process is of higher quality and more homogenous, which could be attributed to the fact that VARTM provides resin impregnation through the micro pores of the concrete as observed in the laboratory during VARTM processing of the samples. As a result, the concrete surface below the adhesive layer no longer remains pure concrete. Its properties would be affected

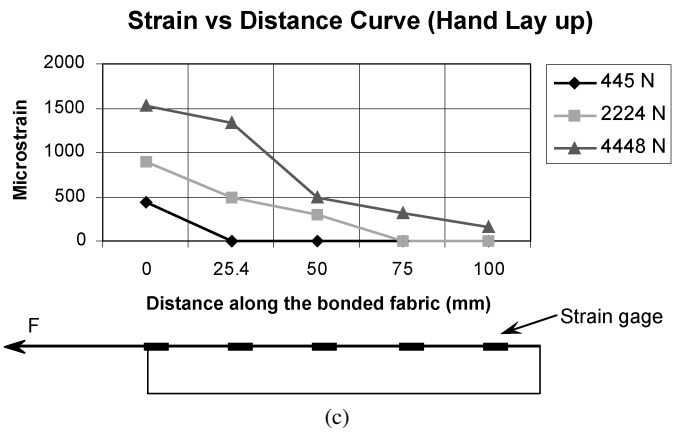

(c)

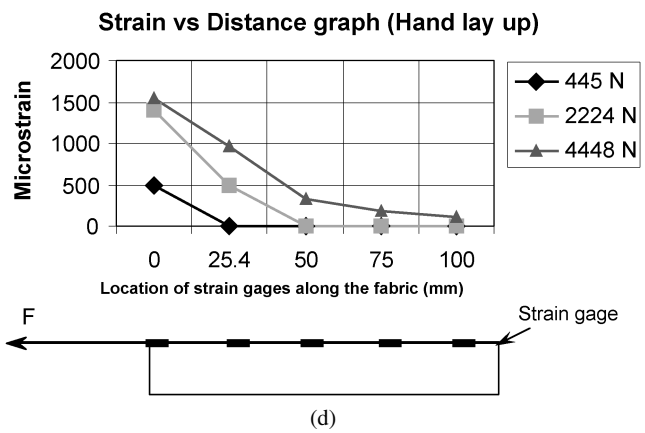

(d)

Figure 15. (Continued.)

Table 3.
Ultimate load in plane testing

Sample	VARTM (N)	Hand lay-up (N)
1	6560	6672
2	5548	5338
3	5773	5604
4	5960	5338
5	5645	5610
6	5835	5746
Mean value	5887	5718
Std dev.	328	451

by the presence of resin, which has a property of higher and brittle type failure load relative to pure concrete. Therefore, as expected, the interface provides a better firm grip to transfer load until a layer of resin impregnated concrete peels out during the

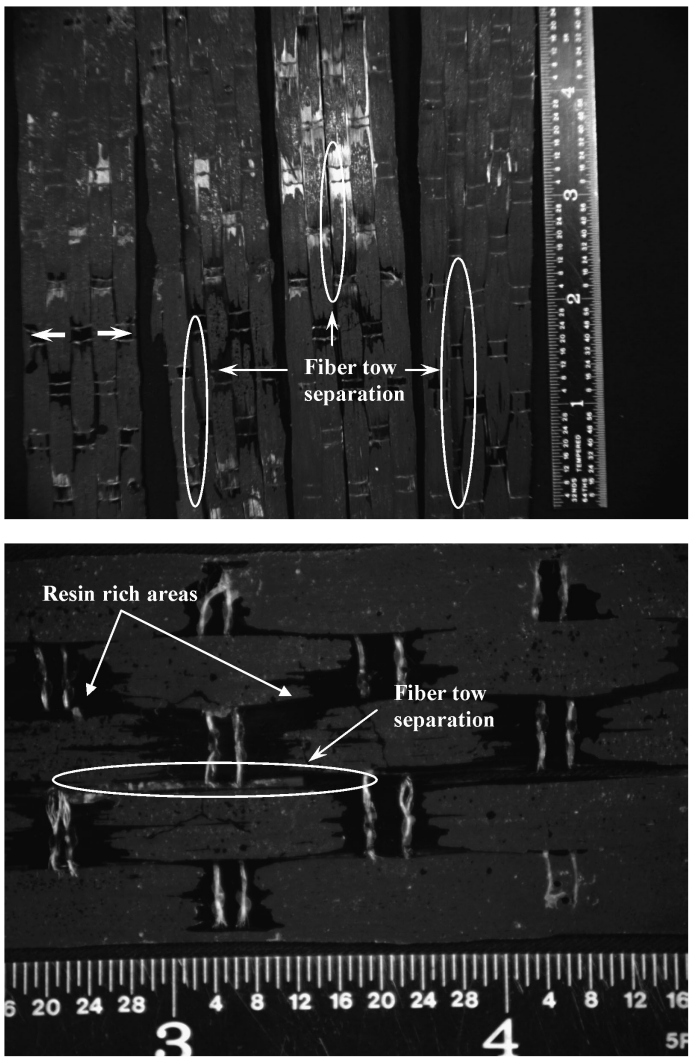

Figure 16. Interfaces obtained in hand lay-up processing after in-plane test. Observe high resin rich areas and interface failure, also observe high shear between fiber tows causes tow separation.

failure. An interface developed in such a way contributes a higher local strain at the loaded end of the CFRP sheet, resulting in shorter load transfer length. So the overall slip value, which is the integration of the FRP strains along the load transfer length, mostly comes from the first region of the loaded end. *In an effort to capture the differences an attempt is made to adjust the available model in the literature. Please note that the proposed adjustment is empirical in nature and only reflects the adjustment necessary to validate the observed experimental results from VARTM processed specimens. It is therefore imperative that more tests are carried out to gain confidence and validate the proposed modifications.*

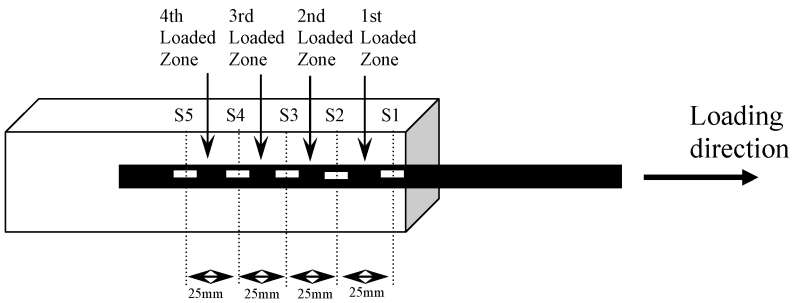

Figure 17. Strategically placed strain gages. S1, S2, S3, . . . , etc. are strain gages.

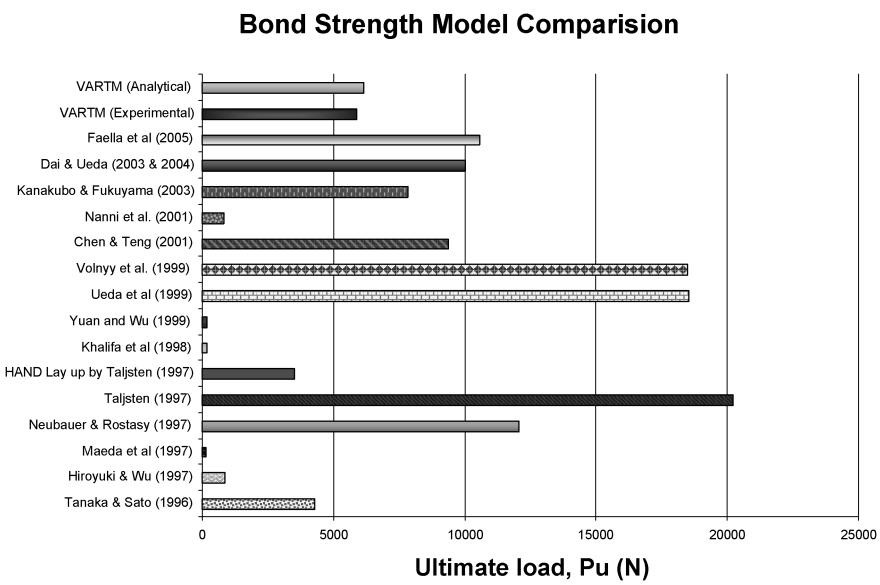

Figure 18. Comparison of existing bond model available in literature with VARTM processed specimens.

For each of the VARTM processed specimens, the bond stress τ *vs* slip diagram corresponding to each value of applied load can be calculated as follows [15]. The bond stress τ can be found by equilibrium of forces considering CFRP linear elastic behavior:

$$\tau(x) = tE\frac{\mathrm{d}\varepsilon_{\mathrm{f}}(x)}{\mathrm{d}x}, \tag{3}$$

where ε_{f} is the CFRP strain. So, the τ *vs* location diagram can be obtained from the first derivative of the strain *vs* location diagram multiplied by the elastic modulus E_{f} and the thickness t_{f} of the CFRP plate. Slip can be calculated as follows:

$$\frac{\mathrm{d}s}{\mathrm{d}x} = \varepsilon_{\mathrm{f}} \tag{4}$$

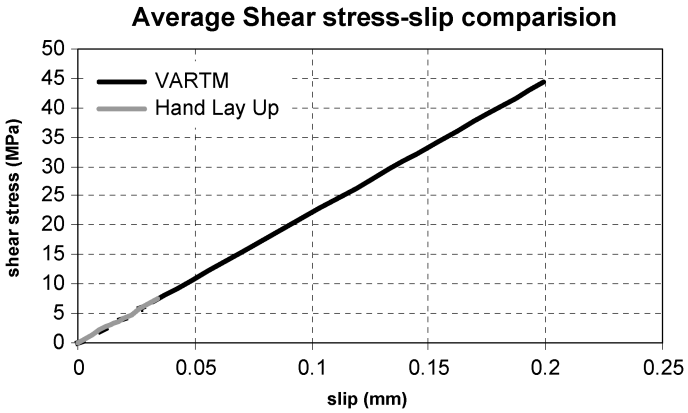

Figure 19. Local τ-slip comparison in-plane shear test for VARTM and hand lay-up processed specimens.

and

$$s(x) = s(0) + \int_0^x \varepsilon_f(x)\,dx, \tag{5}$$

where $s(0)$, the slip at the free end of the CFRP sheet, can be assumed zero prior to peeling. The slip *vs* location diagram can be obtained by integrating the strain *vs* location curve. Figure 19 shows average τ *vs* slip relation as obtained in the experiments. The curve shows linearly ascending trend before the occurrence of interfacial fracture and the value of shear stress suddenly drops to zero when the value of slip exceeds δ_{max} (maximum slip) without demonstrating any softening behavior.

From Fig. 13, it was observed that the strain distribution shows a bilinear behavior at the ultimate stage. The strain gradient, $d\varepsilon/dx$ of the linear curves is more or less the same for all the specimens and maximum in the first loaded region between 0–25.4 mm. Therefore, it was assumed that this 0 to 25.4 mm zone was an effective bond strength transfer zone for this type of specimen, as strain profiles reach zero after this zone. The average calculated gradient in the specimens was 465 μ/mm.

Bond strength developed in this process can be obtained by using non-linear fracture mechanics [11] as shown by the equation (6). The theoretical derivation of this formula was confirmed by other researchers, Wu *et al.* [17] and Dai and Ueda [26]:

$$P = b_f\sqrt{2E_f t_f G_f}, \tag{6}$$

where G_f is the fracture energy per unit area of the joint and can be calculated from area under the τ-slip curve and can be defined using (Blaschko *et al.* [19]):

$$G_f = C_F k_p^2 f_{ctm}, \tag{7}$$

where f_{ctm} is concrete surface tensile strength determined in a pull-off test according to DIN 1048 (1991), C_F is a constant factor with a magnitude equal to 1.59×10^{-3} determined from linear regression analysis of the results of in-plane

shear test, and k_p is a geometric factor related to the widths of bonded plate b_p (mm) and concrete specimens b_c (mm) as follows:

$$k_p = \sqrt{1.125\left(\frac{2 - b_p/b_c}{1 + b_p/400}\right)}. \tag{8}$$

Figure 18 demonstrate a significant improvement of interfacial fracture energy for VARTM over the hand lay-up processed specimens, which can be explained by the fact that more energy is required to bring a local bond element to shear fracture (debonding) in a VARTM processed specimen. Therefore, an interfacial improvement constant k_{imp} of the average surface tensile strength of concrete is introduced in the equation (7) for VARTM strengthened specimens to reflect the observation and the equation (7) becomes:

$$G_{f\_Vartm} = C_F k_p^2 k_{imp} f_{ctm}, \tag{9}$$

where E_f has unit in MPa; and t_f in mm.

The average test value of surface tensile strength for VARTM strengthened specimens over the hand lay-up from the experiments, k_{imp} was 33.6 ($k_{imp} = G_{f\_Vartm}/G_{Handlayup} = 33.6$), and the effective bond length, L_e can be taken as 25 mm.

In comparison, for example, the ultimate load in the experiment and the ultimate load calculated are reasonably close (e.g. average value of experimental results of each sample in Table 3 is 5887 N *vs* 6163 N as predicted from the model). Therefore, the model can predict the experimental results closely. However, more experimental results are necessary to refine the constant K_{imp} and equation (9).

4. Conclusions

By summarizing the work covered in this paper the following conclusions can be reached.

The influence of surface preparation of concrete has been shown to make a profound effect in the measured superficial substrate strength, due to irregularities and air inclusions in substrate.

The effect of the VARTM processing on the bond strength is positive and shows the development of a carbon–concrete interface more homogeneous than the one found by traditional hand lay-up methods. The experiment on the other hand, has shown a very similar overall trend in bond strength for the VARTM and hand lay-up processed specimens. This is not surprising mainly due to the scale effect of FRP strip used for both processing cases. It is perhaps unrealistic to expect a significant difference in ultimate load between the two processes with such a small application of CFRP on a concrete prism especially when both processes were performed in the laboratory. It can however, be extrapolated that in large scaled-up and practical applications of CFRP, resin rich areas and tow separation typical of the hand lay-up process as observed in this study could provide a significant advantage to VARTM

over the hand lay-up. Moreover, life cycle expectancy and maintenance costs due to better consolidation of CFRP (hence a better quality product) can also ultimately give competitive advantages to VARTM over hand lay-up.

Finally, a non-linear fracture mechanics based bond strength model (Taljsten [11]) was modified to predict the VARTM processed experimental results. The Taljsten [11] model could realistically predict the ultimate load at which de-bonding occurs. However, more test results are needed to refine the model. In addition, the results obtained from the in-plane shear test correspond the beginning of an interface characterization process, that can be followed up by an out-of-plane response study.

Acknowledgements

The authors gratefully acknowledge funding and support provided by Alabama Department of Transportation ALDOT research project 930-549 under the guidance of Bridge Engineers, Fred Conway and George Connor.

References

1. H. K. Lee and L. R. Hausmann, Structural repair and strengthening of damaged RC beams with sprayed FRP, *Compos. Struct.* **63**, 201–209 (2004).
2. O. Hang-Elsafi, S. Alampalli and J. Kunin, Application of FRP laminates for strengthening of a reinforced concrete T-beam bridge structure, *Compos. Struct.* **52**, 453–466 (2001).
3. M. N. S. Hadi, Retrofitting of shear failed reinforced concrete beams, *Compos. Struct.* **62**, 1–6 (2003).
4. O. Rabinoitch and Y. Frostig, Experimental and analytical comparison of RC beams strengthened with CFRP composites, *Composites, Part B: Engng* **34**, 663–677 (2003).
5. M. J. Chajes, W. W. Finch, Jr., T. F. Januszka and T. A. Thomson, Jr., Bond and force transfer of composite materials plates bonded to concrete, *ACI Struct. J.* **93**, 208–217 (1996).
6. H. Yoshizawa, T. Myojo, M. Okoshi, M. Mizukoshi and H. S. Kliger, Effect of sheet bonding condition on concrete members having externally bonded carbon fiber sheet, in: *4th Mater. Engng Conf.*, ASCE Annual Convention, Washington, DC, USA (1996).
7. T. Horiguchi and N. Saeki, Effect of test methods and quality of concrete on bond strength of CFRP sheet, *Non-Metallic (FRP) Reinforcement for Concrete Structures*, vol. 1, pp. 265–270. Japan Concrete Institute, Japan (1997).
8. K. Brosens and D. Van Gemert, Anchoring stresses between concrete and carbon fiber reinforced laminates, *Non-Metallic (FRP) Reinforcement for Concrete Structures*, vol. 1, pp. 271–278. Japan Concrete Institute, Japan (1997).
9. T. Maeda, Y. Asano, Y. Sato, T. Ueda and Y. Kakuta, A study on bond mechanism of carbon fiber sheet, *Non-Metallic (FRP) Reinforcement for Concrete Structures*, vol. 1, pp. 179–286. Japan Concrete Institute, Japan (1997).
10. M. Xie and V. M. Karbhari, Peel test for characterization of polymer composite/concrete interface, *J. Compos. Mater.* **18**, 1806–1818 (1997).
11. B. Taljsten, Plate bonding: strengthening of existing concrete structures with epoxy bonded plates of steel or fiber reinforced plastics, *Doctoral Thesis*, Luleå University of Technology, Sweden (1994).

12. B. Taljsten, Defining anchor lengths of steel and CFRP plates bonded to concrete, *Intl. J. Adhes. Adhes.* **17**, 319–327 (1997).
13. L. Bizindavyi and K. W. Neale, Transfer lengths and strengths for composites bonded to concrete, *J. Compos. Construct., ASCE* **3**, 153–160 (1999).
14. V. A. Volnyy and C. P. Pantelides, Bond length of CFRP composites attached to precast concrete walls, *J. Compos. Construct. ASCE* **3**, 168–176 (1999).
15. A. Nanni, D. Lorenzis and B. Miller, Bond of FRP laminates to concrete, *ACI Mater. J.* **98**, 256–264 (2001).
16. J. F. Chen and J. G. Teng, Anchorage strength models for FRP and steel plates attached to concrete, *J. Struct. Engng, ASCE* **127**, 784–791 (2001).
17. Z. S. Wu, H. Yuan and H. D. Niu, Stress transfer and fracture propagation in different kinds of adhesive joints, *J. Engng Mech., ASCE* **128**, 562–573 (2002).
18. V. Karbhari, M. Engineer and D. A. Eckel II, On the durability of composite rehabilitation schemes for concrete: use of a peel test, *J. Mater. Sci.* **32**, 147–156 (1997).
19. M. Blaschko, R. Niedermeier and K. Zilch, Bond failure modes of flexural members strengthened with FRP, in: *Proc. 2nd Intl Conf. Compos. Infrastruct. (ICCI 1998)*, H. Saadatmanesh and M. R. Ehsani (Eds), Tucson, Arizona, USA, pp. 315–327 (1998).
20. H. Toujanji and G. Ortiz, The effect of surface preparation on the bond strength of concrete, *Compos. Struct.* **53**, 457–462 (2001).
21. J. G. Teng, J. F. Chen, S. T. Smith and L. Lam, FRP Strengthened RC Structures, 1st edn, pp. 11–27. J. Wiley and Sons, Chichester, UK (2002).
22. W. D. Brouwer, D. C. F. C. Van Herpet and M. Labordus, Vacuum injection moulding for large structural applications, *Composites Part A: Appl. Sci. Manufact.* **34**, 551–558 (2003).
23. O. Buyukoztur and B. Hearing, Failure behavior of precracked concrete beams retrofitted with FRP, *J. Compos. Construct., ASCE* **2**, 138–144 (1998).
24. J. C. Serrano-Perez, Implementation of vacuum assisted resin transfer molding (VARTM) technology in the repair of reinforced concrete structures, *Master of Science Thesis*, University of Alabama at Birmingham, USA (2003).
25. Sika, *Construction Products Catalog* C160, Sika Corporation, USA (2002).
26. J. G. Dai and T. Ueda, Local bond stress slip relations for FRP sheets — concrete interfaces, *FRPRCS-6*. Singapore (2003).